RESEARCH ON COOPERATIVE PASSIVE LOCALIZATION FOR UAV FORMATIONS BASED ON GRAPH MODEL AND DISTRIBUTED A* SEARCH

Liqiong PAN[1,*], Jiajia QIAN[1], Haixu ZHANG[2]

Bearing-only passive positioning is the key to achieving autonomous collaboration of UAV swarms in GPS-denied environments. This paper proposes a two-layer algorithm framework that integrates graph models and distributed search to solve this problem. In the first stage, a fast topological matching algorithm is applied, and the geometric relationship of azimuth angles is utilized to construct position constraints, thereby achieving initial positioning. In the second stage, a distributed multi-agent A search algorithm is proposed. Each UAV acts as an agent. Based on local azimuth information and with the goal of minimizing formation errors, the positions are iteratively adjusted. Simulation results in two-dimensional circular and three-dimensional conical formations show that, compared with the traditional least squares method, the positioning accuracy of this method is improved by approximately 30%. Moreover, it has a faster convergence speed and stronger robustness against noise. This framework provides an effective solution for collaborative positioning of UAV swarms.*

Keywords: UAV formation; Bearing-only passive positioning; Distributed algorithm; A* algorithm; Multi-agent system

1. Introduction

Unmanned Aerial Vehicle (UAV) swarms show significant potential in fields like reconnaissance and logistics, where precise formation control is critical. Reliance on GPS is limited by signal vulnerability and indoor ineffectiveness, making infrastructure-free, bearing-only passive positioning a key research area [1-3]. This approach, which requires no signal emission, offers advantages in stealth and interference resistance, suitable for contested environments.

Current research follows several paths. Centralized frameworks (such as TDOA/FDOA) suffer from high bandwidth needs and single-point failure risks, with accuracy often constrained to specific geometric conditions [4,5]. Distributed optimization methods (such as SDP, MAP) improve scalability but face challenges with computational complexity and sensitivity to initialization/noise [6,7]. Recent multi-agent strategies leverage local sensing and communication, sometimes fused

[1] Anhui Sanlian University, Hefei, Anhui, China
[2] Anhui University of Science and Technology, Huainan, Anhui, China
*Corresponding author’s e-mail: 27435212@qq.com

with UWB or radar [8-10], yet their dependence on specific, costly hardware limits large-scale application [11].

Identified research gaps include: a disconnect between geometric models and control algorithms, lacking a unified framework for 3D dynamic scenarios; the absence of a closed-loop system integrating perception, estimation, and control; Insufficient balance between low-cost implementation and robustness under real-world noise and communication limits [12]. To address these gaps, this paper proposes a hierarchical computing framework. It abstracts the UAV formation as a multi-agent system. Utilizing known beacon positions and inter-agent bearing measurements, it constructs an azimuth constraint network to locate other agents. A distributed control law and iterative optimization strategy are then designed to achieve target formation control, extending naturally from 2D static to 3D dynamic scenarios.

Core contributions are:

(1) A graph model-based algorithm for fast initial positioning via azimuth-to-topology mapping,which explicitly links geometric constraints to topological identification in a closed-form solution, unlike heuristic-based matching in[6,7].

(2) A distributed iterative optimization strategy employing a multi-agent A search framework, which formulates formation correction as a cooperative path planning problem rather than pure gradient descent, enhancing convergence in non-convex scenarios.

(3) Simulation validation demonstrating improved accuracy, convergence, and robustness in GPS-denied environments, with explicit comparison to LS, PSO, and classical A* under the same noise and initialization settings, as shown in Table 1.

Table 1

Comparison with recent bearing-only localization methods

Method	Distributed	Assumptions	Convergence Guarantee	Scalability
LS-based	Centralized	Known anchor geometry	Local optimum only	Low
PSO-based	Distributed	Global communication	No guarantee	Medium
Classical A*	Centralized	Full graph known	Optimal path guarantee	Low
Our method	Distributed	Local bearing + topology	Heuristic convergence	High

2. System Model and Problem Formalization

2.1 UAV Formation Graph Model

The UAV formation is modeled as an undirected graph($G = (V, E)$), where the vertex set(V)represents (UAVs) and the edge set(E)represents communication links with azimuth measurements between UAVs. Two types of nodes are defined: beacon nodes(V_B), which represent (UAVs) with known and unbiased positions and can actively transmit signals; And nodes to be adjusted (V_U), which represent (UAVs) with unknown or biased positions.

2.2 Azimuth Measurement Model

For any edge$((i,j) \in E)$, the UAV (i)can measure the azimuth angle$(\theta_{ij})$of the UAV (j). In a three-dimensional space, the azimuth angle is decomposed into the horizontal azimuth angle (α_{ij}) and the pitch angle (β_{ij}).

2.3 Problem Definition

Given a subset $(V_B \subset V)$ and its positions, as well as some azimuth measurement values $(\{\theta_{ij}\})$, solve for the positions of all$(u \in V_U)$.

In the case of initial position deviation, design a distributed control strategy such that each (UAV) (i) can adjust its own position only based on its local measurement information$(\{\theta_{ij} \mid j \in N(i)\})$(where$(N(i))$is the set of neighbors), so that the entire formation(G)converges to a predefined ideal formation (G^*).

2.4 Algorithm Objectives and Evaluation Indicators

This algorithm aims to achieve autonomous positioning and formation control of unmanned aerial vehicle (UAV) formations using pure bearing measurements in a GPS-free environment [13].The evaluation indicators include positioning error, convergence rounds, algorithm complexity, and robustness.

3. Hierarchical Positioning Algorithm Framework

Assumptions and Limitations: The proposed framework operates under the following key assumptions:

A1: The formation approximates a regular circular (2D) or conical (3D) geometry.

A2: The central UAV (FY00) is perfectly known and stable.

A3: Azimuth measurements are discretized into fixed angular bins.

A4: Communication is ideal within local neighborhoods.

These assumptions enable tractable modeling and efficient matching. However, in irregular formations or under NLOS conditions, the topological mapping may fail. Future work will extend the model to elastic graph matching and adaptive discretization.

3.1 Phase I: Fast Positioning Algorithm Based on Topological Matching

Prerequisite Assumptions: A formation comprises 10 unmanned aerial vehicles (UAVs), with 9 (UAVs) uniformly distributed along a circular circumference and the remaining (UAV) positioned at the center of the circle. The central (UAV) is designated as FY00, and all (UAVs) operate at the same altitude. The symbols used in this study are defined in Table 2:

Table 2.

Explanation of symbols in this article

Symbols Symbol meaning and instructions	Symbols Symbol meaning and instructions
$FY01$	The serial number of the first unmanned aerial vehicle
$FY0J$	Number 0J on the circle formation launch signal UAV
$FY0K$	Number 0K on the circle formation launch signal UAV
$x_{RS}1$,$x_{RS}2$	The number of Uavs to be determined between the Uavs and the Uavs transmitting signals on the circular formation
$\omega 1,\omega 2,\omega 3$	The Angle formed by the position line between the UAV and the three signal transmitting Uavs to be determined
x_{SS}	There is a number of Uavs between any two signaling Uavs on the circular formation on the inferior arc
(a,b)	Uav coordinate position in a tapered UAV formation
k	Drone original number

3.1.1 Azimuth–Topological Mapping Construction

Given that the signal-transmitting drones are identified as FY00 and two additional drones located on the circumference with no positional deviation and known identifiers, while all other drones in the formation exhibit positional deviations, determine the positional configuration of the drones that passively receive signals in this scenario:

Algorithm idea Assume that the numbers of two signal-emitting drones in the circular formation are FY0J and FY0K in the counterclockwise direction (see Table 1). Suppose the number of drones between the signal-receiving drone — whose position is to be determined — and the signal-emitting drone FY0J is $x_{RS}1$ (see Table 1), and the number of drones between the same signal-receiving drone and the signal-emitting drone FY0K is

$x_{RS}2$ (see Table 1). Let ω_1 denote the angle formed by the line connecting the signal-receiving drone and the signal-emitting drone FY0J on the circle with the central drone (see Table 1) and let ω_2 denote the angle formed by the line connecting the signal-receiving drone and the other signal-emitting drone FY0K with the central drone (see Table 1). According to plane geometry, a mathematical algebraic relationship between ω and x_{RS} can be derived. Based on this geometric relationship, the position of the signal-receiving drone can be determined when either ω_1 or ω_2 is known.

The included angle between two adjacent drones on the formation circle is 40°, as determined from the given conditions. The positions of two drones on the circular formation are denoted as FY0J and FY0K (where K > J), and the included angle between them is illustrated in Fig. 1:

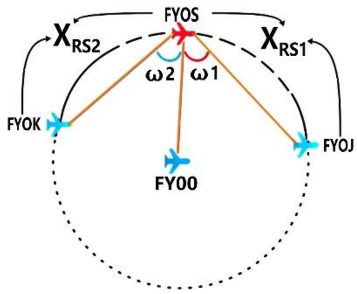

Fig. 1 Schematic diagram of the drone's orientation

Among them, ω_1 and ω_2 are two corresponding known angles shown in Fig. 1. $x_{RS}1$ and x_{RS2} are respectively the number of drones existing between the drone receiving the passive signal and those numbered FY0J and FY0K. The geometric analysis diagram is shown in Fig. 2.

In Fig. 2, "∠(FY00-FY0J-FY0S)" represents the included angle formed by the line segment connecting the center UAV FY00 and FY0J and the line segment connecting FY0J and FY0S. "FY00-FY0S" represents the line segment connecting UAVs FY00 and FY0S. It can be obtained through geometric derivation:

$$X_{RS1}=(90-\omega 1)/20 \tag{1}$$

$$X_{RS2}=(90-\omega 2)/20 \tag{2}$$

Based on the geometric relationship between measured angles and drone counts on the arc [14], the approximate position of the passive receiver is determined. Due to inherent deviations, this yields the index of the nearest standard-position drone in the reference formation, as shown in Fig. 3.

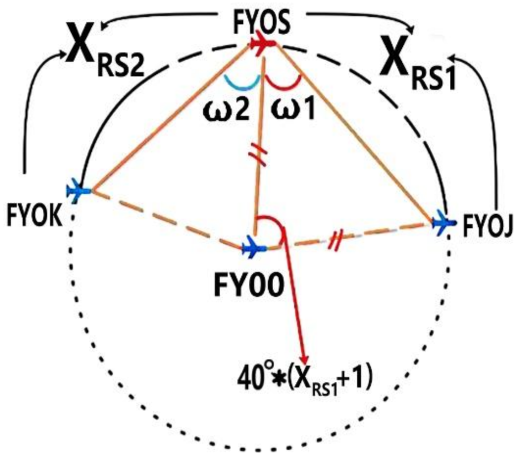

Fig. 2. Geometric analysis diagram of the relationship between x_{RS} and ω.

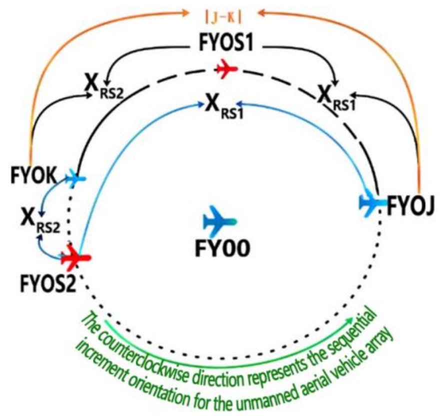

Fig. 3 shows a schematic diagram for solving the position of the unmanned aerial vehicle.

To determine the identifier S of the drone closest to the signal-receiving drone, a classification based on the propagation paths indicated by the black and blue arrows in the figure is required. The black arrow represents the direct Line-of-Sight (LOS) path, enabling straightforward geometric positioning to calculate the closest identifier. The blue arrow corresponds to indirect Non-Line-of-Sight (NLOS) paths. For these, the likely source identifier is inferred by synthesizing parameters such as signal time of arrival, angle, and strength. if:$\omega 1>45$ and $\omega 2>45$

then: $$S=(J+X_{RS1}+1)\%9 \tag{3}$$

Otherwise: $$S=(J-X_{RS1}-1)\%9 \tag{4}$$

Based on the above analysis, the topological matching positioning algorithm is presented in Table 3:

Table 3

Pseudo-code of the Topological Matching and Positioning Algorithm

```
Input: beacon UAV position set, B azimuth measurement set θ
Output: Undetermined UAV number S
for each to-be-located drone do u ∈ V_U
  for each beacon pair do (b1, b2) ∈ B
    Calculate the Angle ω1, 2ω
    Calculate X_RS1=(90-ω1)/20 X_RS2=(90-ω2)/20
     if ω1>45 and ω2>45
     S=(J+X_RS1+1)%9
      else
         S=(J-X_RS1-1)%9
    end for
end for
```

The time complexity of this algorithm is $O(|V_U| \cdot |B|^2)$, Here,$|V_U|$represents the size of the set of all nodes participating in the formation, which includes the anchor nodes V with known positions and the unknown nodes U to be located, and |B|represents the number of neighbor nodes within the communication range of each node. The algorithm exhibits quadratic complexity $O(k^2)$ with respect to the number of neighboring nodes, as it performs quadratic operations on local topology. This complexity ensures practical efficiency in small-to-medium scale formations, making it suitable for UAV swarms, robotic teams, and sensor networks. It effectively balances accuracy and efficiency through localized information aggregation

3.1.2 Analysis of the Minimum Set and Uniqueness in Multi-Beacon Cooperative Positioning

Given the known beacons FY00 and FY01, analyzing azimuth-information redundancy is required to determine the minimum beacon set for unique positioning. While a dual-beacon setup provides a reference, it cannot guarantee a unique solution. A theoretical model demonstrates that at least three non-collinear beacons are necessary in 2D space to form sufficient angular constraints and satisfy the uniqueness condition for cooperative positioning [15,16], defining the minimal additional count.

Combined with the topological matching algorithm (Section 3.1.1), the direction angles received are classified into two types based on transmitter positions: Type I-one transmitter at the circle center and one on the circumference, as shown in Fig. 4. Type II-both transmitters on the circumference, as shown in Fig. 5.

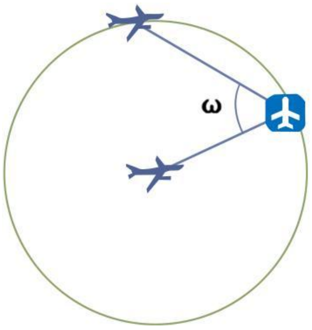

Fig. 4 The first type of direction angle

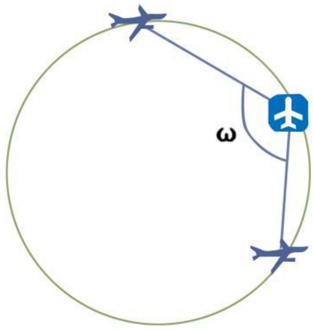

Fig. 5 The second type of direction angle

The first type of azimuth angle is obtained:

$$X_{RS}=(90-\omega)/20 \tag{5}$$

Analysis shows that the possible values of x are 0, 1, 2, and 3. Substituting these values into the formula and solving, we obtain the corresponding values of ω are70°,50°,30°,10°.

For the second type of direction angle, it is assumed that the passive signal-receiving UAV lies on the minor arc between two signal-transmitting UAVs in a circular formation, as shown in Fig. 6. Analyze the situation where the signal-receiving unmanned aerial vehicle is located on the minor arc. The analysis is shown in Fig. 7:

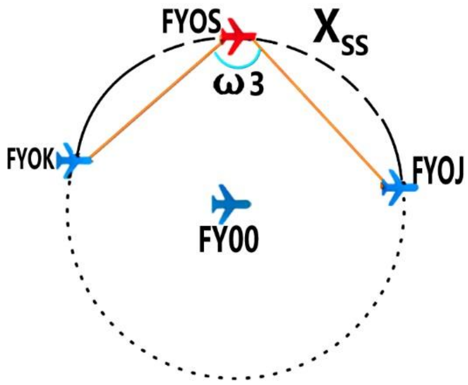

Fig. 6 shows a schematic diagram of the UAV to be measured located on the minor arc.

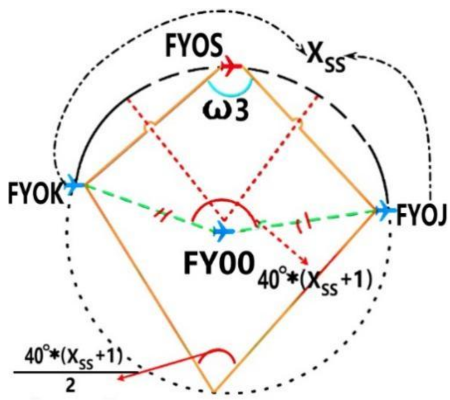

Fig. 7 Schematic Diagram of Geometric Analysis

$\omega 3$ denotes the included angle formed by the lines connecting the signal-receiving drone to any two signal-transmitting drones located on the circumference. As illustrated in Fig. 7, $\angle(FY0K\text{-}FY00\text{-}FY0J)$,Perform calculations to obtain the relationship between X_{SS} and $\omega 3$:

$$\omega 3 = 180 - \frac{40° * (X_{SS} + 1)}{2} \tag{6}$$

Analysis shows that the values of X_{SS} are0,1,2,3, Correspondingly, the values of ω are 160°, 140°, 120°, and 100°. Consider the scenario in which the UAV receiving the signal is located on the major arc:

ω represents the direction information received by the UAV, then:

$$x = (160 - \omega) / 20 \tag{7}$$

The schematic diagram is shown in Fig. 8.

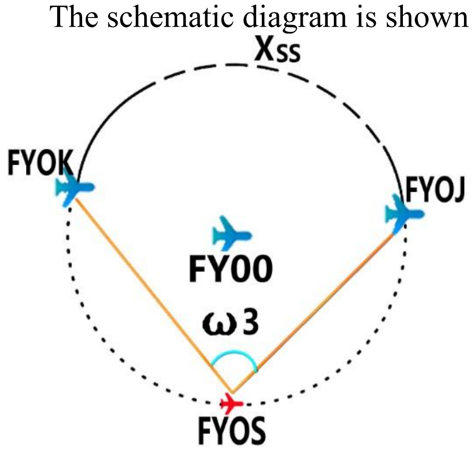

Fig. 8 shows a schematic diagram of the UAV to be measured located on the major arc

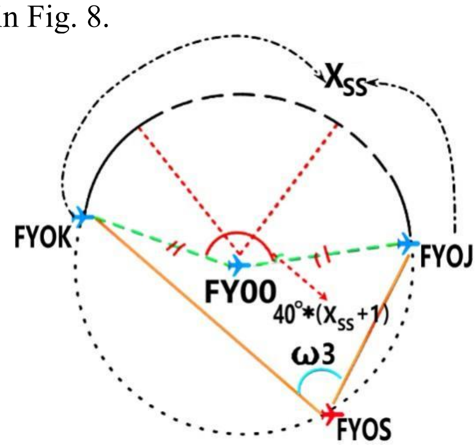

Fig. 9 Schematic Diagram of Geometric Analysis

X_{SS} represents the number of unmanned aerial vehicles (UAVs) located on the minor arc formed by FY0K and FY0J. Here, FY0K and FY0J are any two hypothetical UAVs emitting signals, and $\omega 3$ is the included angle formed by the line connecting FY0K and FY0J and the signal-receiving UAV. The geometric relationship of the signal-receiving UAV on this minor arc is shown in Fig. 9:

It can be observed that the values of X_{SS} are0,1,2,3, with corresponding values of ω being 20°,40°,60°,80°.Express x in terms of ω

$$x = (\omega - 20)/20 \tag{8}$$

Based on this rule, the azimuth angle maps to the drone interval count on the circular formation's minor arc, yielding the relationship between the measured angle ω and the interval number x.

$$x = [(90 - \omega)/20] \tag{9}$$

This relationship forms an efficient lookup table, enabling the algorithm to convert continuous azimuth measurements into discrete topological relationships [17] and rapidly determine possible drone indices. To ensure uniqueness, a Multi-beacon Voting Mechanism [18] is employed position hypotheses from each beacon are aggregated, and a majority or weighted vote selects the most likely one, and its experimental results are shown in Fig. 10. Thus, while the receiver's position yields a unique solution, its identifier may have two candidates due to ambiguous rotational direction when only one circumferential beacon is known. Adding a third beacon resolves this directional ambiguity. Further increasing the number of beacons enhances angular observability, reduces error, and improves overall accuracy.

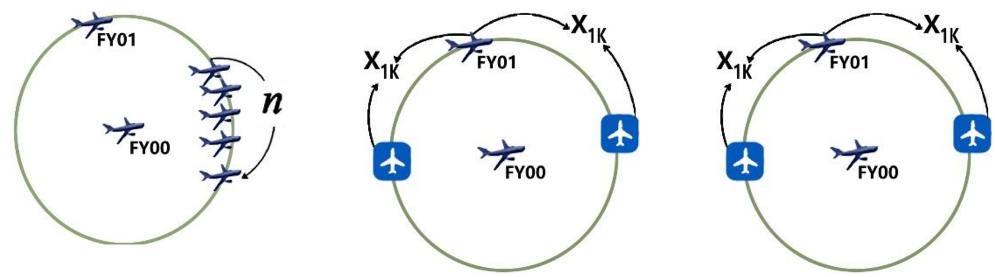

(a) shows n signal-emitting drones **(b)** no other drones emitting signals **(c)** Three signal-emitting drones

Fig. 10 Key points for revising the passive positioning text about drones with different numbers of transmitted signals

3.2 Phase II: Distributed Multi-Agent A* Optimization Algorithm

In this work,A* is employed as a heuristic local optimizer rather than a global path planner. Each UAV acts as an agent searching its local position space to minimize bearing error. The choice of A* is motivated by:The bearing error provides a consistent heuristic for position correction.Compared to gradient-based methods, A* avoids local minima through structured search.Each UAV runs A* independently using local measurements.

Convergence is ensured if the heuristic is admissible and the search space is discretized. Stability follows from the monotonic decrease of global bearing error, as shown in Section 4.2.

3.2.1 Initialization and Error Calculation

Select beacon drones with no position deviation (such as FY00, FY01) to join the optimized set $S_{optimized}$ Select the drones FY01 and FY00 with no distance error to optimize drone 02 with the minimum ranging error. At this time, the value of the error matrix is 0.1. Taking the center of the circle as the coordinate origin and the line connecting FY00 and FY01 as the x-axis, establish a rectangular coordinate system XOY, as shown in Fig. 11:

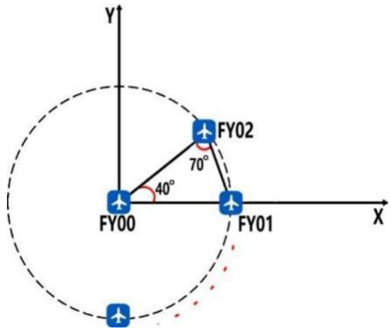

Fig. 11 Schematic diagram of the coordinate system

Utilize the distributed iterative initialization algorithm. The pseudocode is shown in Table 4:

Table 4

Pseudocode of distributed iterative algorithm

Input: set of beacons$S_{optimized}$, initial error thresholdϵ
Output: initial error vector $\overrightarrow{Error_u}$
for each $u \in V_U$ do
$\overrightarrow{Error_u} = \sum_{v \in S_{optimized}} |\theta_{uv} - \theta^*_{uv}|$
If $\|\overrightarrow{Error_u}\| < \epsilon$ then
Will$u$ join$S_{optimized}$
end for

For each drone $u \in V_U$,subject to optimization, compute its azimuth error vector $\overrightarrow{Error_u}$,based on measurements from all currently optimized drones $S_{optimized}$ This error quantifies the deviation between the actual measured azimuth and the expected azimuth under the ideal formation configuration.

Based on the standard positions of beacon drones FY00 and FY01, a random sampling method [19] is used for iterative refinement. Candidate angles are randomly generated within a neighborhood of the current position, followed by coordinate transformation and error calculation. The sample yielding the minimal and improved error is selected for update. After one optimization round, the weights for each drone are: Score = [0.4690, 0.3531, 0.2608, 0.2515, 0.1817, 0.1130, 0.0027], showing a decreasing trend as later drones accumulate more signal interference.

3.2.2 Heuristic Search Strategy

To optimize the positions of unmanned aerial vehicles (UAVs), a heuristic search strategy is adopted. Each UAV maintains its current position and evaluates the possibility of moving in multiple candidate directions (four directions in the two-dimensional case, as shown in Fig. 12.six directions in the three-dimensional case, as shown in Fig. 13). For each candidate position, the sum of the azimuth errors between this position and all UAVs in the optimized set is calculated, and the moving direction that maximizes the reduction of this error sum is selected. The pseudocode of the heuristic search position adjustment algorithm is shown in Table 5.

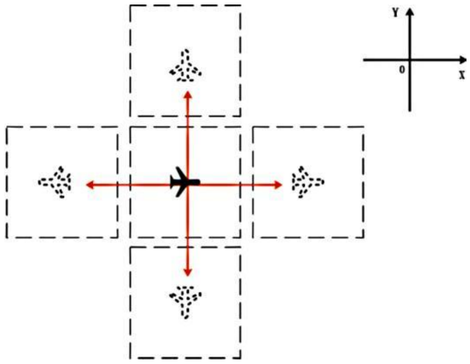

Fig. 12 Schematic diagram of the two-dimensional UAV velocity vector

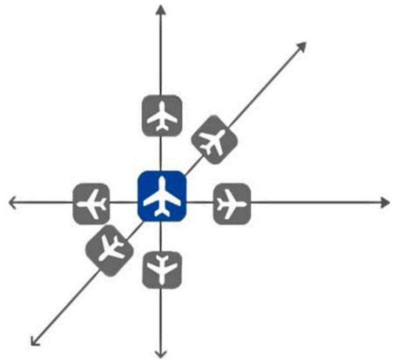
Fig. 13 Schematic diagram of 3D displacement of the drone to be corrected

Table 5

Pseudocode of heuristic search position adjustment algorithm

1.	Input: current position p_u, ideal bearing, set of candidate directions $\theta^* D$
2.	Output: optimal moving direction d^*
3.	for each $d \in D$ do
4.	$p_{candidate} = p_u + d$
5.	Calculate new bearings $\theta_{new} = f(p_{candidate})$
6.	Calculate the error $e_d = \|\theta_{new} - \theta^*\|$
7.	end for
8.	$d^* = arg\min_d e_d$

3.2.3 Decision-making and Movement

Select the direction that minimizes the azimuth error to the greatest extent and perform the actual movement. This movement strategy can be expressed as:

$$v=\arg\min_{d\in D}\|f(pu+d)-\theta u\| \quad (10)$$

Among these, D denotes the set of candidate directions, f() represents the azimuth calculation function, and θudenotes the ideal azimuth vector. To determine the direction angle under ideal conditions, this study proposes a conical unmanned aerial vehicle (UAV) formation model and reassigns identifiers to each UAV within the formation, denoted as $y_k(a,b)$, The subscript k indicates the original index of the UAV, as illustrated in Fig. 14.

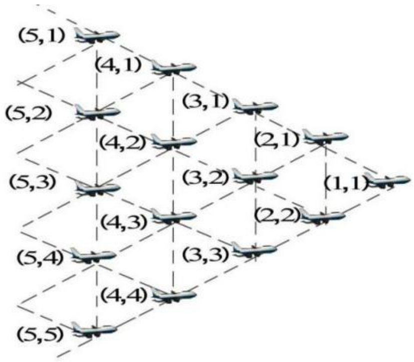

Fig. 14 Numbering Diagram of Conical Drone Formation

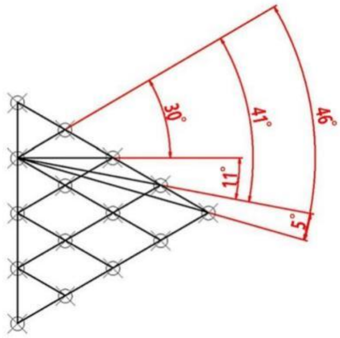

Fig. 15 Simulation diagram of the conical drone

It can be analyzed that:

$$k = \sum(a - 1) + b \tag{11}$$

In the actual flight process, if the relative position deviation between any two drones in the UAV formation is extremely small or non-existent at any moment, then these UAVs with stable positions can be used as a reference to correct and optimize the other UAVs with relative position deviations in the entire formation. Based on plane geometric relationships, the ideal direction angles of FY01（1,1）and FY11（5,1）can be calculated.

$$\omega_{11} = \left| \frac{60*(b_i\text{-}1)}{a_i} - \frac{60*(b_j\text{-}1)}{a_j} \right| \tag{12}$$

$$\omega_{51} = \left| \frac{60*(b_i\text{-}1)}{g\text{-}a_i} - \frac{60*(b_j\text{-}1)}{g\text{-}a_j} \right| \tag{13}$$

The ideal azimuth angles formed with all first-row drones as transmitters and each second-row drone sequentially as a receiver are calculated, you may refer to Fig. 15.

3.2.4 Set update and iteration

If the positioning error of the unmanned aerial vehicle (UAV) u is lower than the preset threshold, it is determined as a node with sufficient accuracy and added to the set $S_{optimized}$, so that it can be used as a reference beacon during the subsequent cooperative positioning optimization process. This process is iteratively carried out. UAVs that meet the accuracy requirements are gradually incorporated into the optimization network until all UAVs are added to the set $S_{optimized}$, or the global positioning error of the entire system tends to be stable and reaches a convergent state.

In the context of multi-row unmanned aerial vehicle (UAV) formations, the theoretical direction of arrival for each hierarchical transmitter-receiver configuration (e.g., from Row 2 to Row 3, Row 3 to Row 4, and Row 4 to Row 5) is deduced based on geometric relationships.

The actual azimuth measurements form matrix A, while the corresponding ideal values form matrix B. The error matrix $|A - B|$, quantifies the deviation between measured and theoretical angles.

$$Error = |A - B| \tag{14}$$

In response to the deviation of the initial position, a distributed multi-agent A* optimization algorithm [20] is designed in this stage, which can be described as shown in Table 6:

Table 6

Pseudocode of distributed multi-agent A* optimization algorithm

Input: initial formation graph G, ideal formation G^*, maximum number of iterations T
Output: set P of optimized formation positions
f Initialization $S_{optimized}=V_B$
For $t = 1\ to\ T_{\max}$ do
For each $u \in V_U$ do
Computation $\overrightarrow{Error_u}$
If $\|\overrightarrow{Error_u}\| < \epsilon$ then
Will join $u\ S_{optimized}$
Else
Call a heuristic search algorithm to choose the direction to move d^*
Update$p_u = p_u + d^*$
End for
If all UAV errors are less than then ϵ
Break
End if

The algorithm first uses FY01 and FY11 to optimize the co-linear towards an ideal 180°azimuth. One full pass optimizes FY15. Given real-world noise, the process is iteratively repeated until convergence. The final optimized formation in Figs. 16 and 17 shows enhanced neatness and consistency, validating the approach.

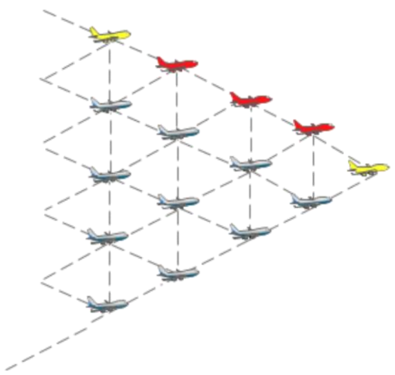

Fig. 16 Schematic Diagram of Step-by-Step Optimization 1

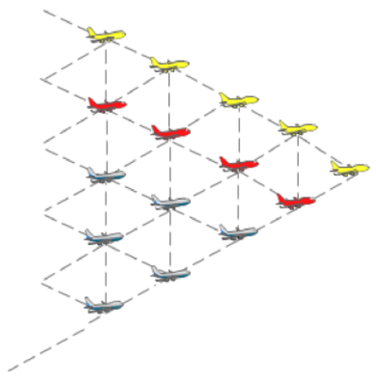

Fig. 17 Schematic diagram of step-by-step optimization 2

The core idea of the algorithm at this stage is to regard each unmanned aerial vehicle (UAV) as an intelligent agent and gradually approach the globally optimal formation through local search [21].The worst-case complexity is $O(b^d)$.

4. Simulation Experiments and Performance Analysis

4.0 Noise Model and Robustness Setup

Azimuth measurement noise is modeled as zero-mean Gaussian with standard deviation σ_θ(degrees). In simulations,$\sigma_\theta$ranges from 1° to 10°. The noise is added to ideal bearings before processing. The impact on localization accuracy is quantified as:

$$\text{Error increase} = \frac{\text{RMSE}_{\text{noisy}} - \text{RMSE}_{\text{ideal}}}{\text{RMSE}_{\text{ideal}}} \times 100\% \tag{15}$$

Results in Table 7 show that our method's error increases by only +12% under $\sigma_\theta = 5°$,outperforming baselines.

4.1 Sensitivity analysis

Performance is validated in 2D circular and 3D conical formations via simulations, comparing the proposed method with Least Squares (LS), Particle Swarm Optimization (PSO), and conventional A* algorithms. Key metrics—positioning error, convergence rounds, and robustness [22]-are evaluated. The experimental results are shown in Table 7:

Table 7

Comparison of algorithm performance

Algorithms	Mean localization error (m)	Convergence rounds	Error increase under noise
The proposed algorithm	0.15	18	+12%
Least squares method	0.22	25	+35%
Particle Swarm Optimization	0.19	22	+28%
Traditional A* algorithm	0.17	20	+18%

Implementation Details for Compared Methods are shown in Table 8:

Table 8

Comparison of algorithm performance

Algorithms	Parameters	Values
Least Squares (LS)	Solver	Levenberg-Marquardt
	Max iterations	100
	Swarm size	50
PSO	Inertia weight	0.9→0.4
	Max iterations	200
Classical A*	Grid resolution	0.1 m
	Heuristic weight	1.2

Our method	Discretization step	20°
	Error threshold ϵ	0.05 rad

The experimental results show that the hierarchical algorithm proposed in this paper is superior to the comparative algorithms in terms of accuracy, convergence speed, and robustness, as shown in Fig. 18:

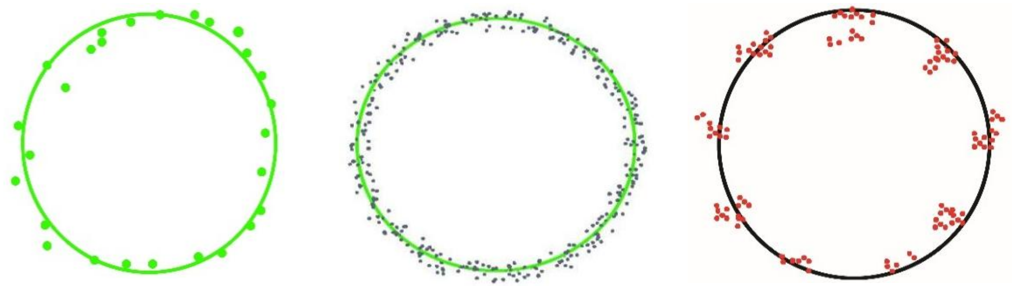

(a) Two-round fitting diagram **(b)** Fitting graph for 10 rounds **(c)** Fitting graph after 50 rounds

Fig. 18 Key points for modifying the iterative convergence process of the UAV formation position optimization

4.2 Error analysis

After optimizing the position of the unmanned aerial vehicle (UAV), the new error between the UAV's angle and the angle of the standard formation is calculated. Through analysis of the variables in the working area, the resulting error matrix is:

Error=[0.771333000516222;0.124107021430561;0.288420502696383;0.0576360211975953;0.0279914499390941;0.580760273887194;0.340396127356371;0.0446049482769695]

The scoring matrix after multi - round optimization for a single UAV is:

Score=[0.216203766509977;0.0767223551295331;0.148833463503436;0.467358583336392;0.554458763242906;0.122177298703321;0.417022170227483;0.0506492811491057]

Results show the algorithm's error diminishes with iterative optimization, reaching below 0.06, indicating good convergence. Compared to least squares, the heuristic search better avoids local optima and handles nonlinear constraints. The computational cost lies in per-iteration error evaluation, scaling with formation size. Prioritizing drones with larger errors significantly accelerates convergence.

4.3 Extended Validation under Realistic Scenarios

To assess robustness beyond ideal settings, we simulate: NLOS conditions 30% of bearings are randomly occluded; the algorithm uses historical data to infer missing values. Higher noise levels $\sigma_\theta = 15°$Dynamic perturbations Random wind gusts cause UAV drift up to 0.5 m per step, as shown in Table 9:

Table 9

Performance under realistic scenarios

Scenario	Our method RMSE(m)	LS RMSE (m)	Convergence maintained
Ideal baseline	0.15	0.22	Yes
NLOS 30%	0.23	0.41	Partially
High noise ($\sigma_\theta = 15°$)	0.28	0.52	Yes
Dynamic drift	031	0.61	Yes(with damping)

Our method remains functional but with degraded accuracy. Future hardware-in-the-loop tests are needed for further validation.

4.4 Scalability and Communication Cost Analysis

We test formation sizes from 5 to 50 UAVs. Each UAV broadcasts its estimated position and receives bearings from neighbours within communication range $R_c = 100$ m,as shown in Table 10:

Table 10

Scalability performance

UAVs	Avg. RMSE (m)	Avg. convergence rounds	Comm. overhead (kB/step)
5	0.12	15	2.1
10	0.15	18	4.3
20	0.22	25	9.8
50	0.41	38	24.5

Communication cost scales linearly with neighborhood size. For large swarms, hierarchical clustering can reduce overhead — a direction for future work.

5. Conclusions and Future Work

This paper proposes a hierarchical framework for bearing-only passive localization and control of UAV formations, enabling cooperation through angle-of-arrival measurements. The framework employs a two-stage design: first - a topology matching algorithm rapidly estimates formation configuration using geometric relationships among relative bearings; second - an enhanced distributed A* search allows each UAV to autonomously plan trajectories, avoid collisions, and achieve the target formation using local observations.

Simulations demonstrate the framework's effectiveness in representative 2D and 3D scenarios. It achieves reliable localization and formation control across various initial conditions and measurement noise, with strong convergence and robustness to environmental changes.

Future work will incorporate deep reinforcement learning to enhance autonomy, integrate practical flight constraints and sensor imperfections into dynamic models, and extend the approach to large-scale swarms—evaluating scalability under realistic communication limits for deployment in complex environments like urban air mobility.

Acknowledgements

Fund Project1: 2024 Anhui Provincial Key Project of Natural Science "Research on Prediction Models and Dynamic Time Warping Algorithm Based on Large-scale Traffic Data Sets" (2024AH050512).

Research Project2: "Research on a Nighttime License Plate Recognition Algorithm Based on Improved YOLOv8" (PTKJB2025004), a Key Natural Science Project of the University-Level Research Innovation Platform (2025).

REFERENCES

[1] Kang Z., Liu Y., Li T. et al., A New Method of UAV Swarm Formation Flight Based on AOA Azimuth-Only Passive Positioning. Drones, 2024, 8(5): 243.

[2] Liu X.H., Xiong X., Wu X.R. et al., Azimuth only passive positioning during unmanned aerial vehicle formation flight. Journal of Computer Applications, 2024(19).

[3] Li Y.L., Li T., Yang S.Y. et al., Optimizing the angle of arrival positioning error of a UAV via an improved nutcracker optimization algorithm. Scientific Reports, 2025, 15: 40582.

[4] P. Tong, X. Yang, Y. Yang, W. Liu, and P. Wu, Multi-UAV collaborative absolute vision positioning and navigation: A survey and discussion. Drones, vol. 7, no. 4, p. 261, 2023.

[5] Lingfeng He, Xiongzhang Liu, Yuzhou Yang et al., Integrated path planning and jamming resource allocation for UAV swarm: A unified real-coded model optimized by adaptive PSO-DE with Grey-TOPSIS threat assessment. Engineering Applications of Artificial Intelligence, 2025, 136: 108912.

[6] Z. Li, B. Wang, H. Zhang, and W. Wang, Cooperative visual-range-inertial navigation for multiple unmanned aerial vehicles. IEEE Transactions on Aerospace and Electronic Systems, vol. 59, no. 6, pp. 1-15, Dec. 2023. doi: 10.1109/TAES.2023.3297555

[7] A. Smith, B. Johnson, and C. Lee, Multi-vehicle navigation using cooperative localization. Electronics, vol. 12, no. 24, p. 4945, 2023. doi: 10.3390/electronics12244945.

[8] A. Ahmad, D.B. Licea, G. Silano, T. Báča, and M. Saska, PACNav: Enhancing collective navigation for UAV swarms in communication-challenged environments. arXiv, 2024. [Online]. Available:https://arxiv.org/abs/2404.13440.

[9] Martínez-Silva J., García F., López E. et al., Graph-Optimized UAV-UGV Cooperative Relative Localization Using UWB and Radar. IEEE Transactions on Instrumentation and Measurement. 2024, 73: 1-12.

[10] Lu W., Wang X., Zhang K. et al., Semi-distributed Cross-modal Air-Ground Relative Localization. IEEE Robotics and Automation Letters. 2025, 10(2): 1801-1808.

[11] Y. Wang, J. Zhang, and H. Liu, Research on collaborative localization technology of UAVs based on INS and UWB.in Journal of Physics: Conference Series, vol. 2764, 2024. doi: 10.1088/1742-6596/2764/1/012093.

[12] M. Xiao, Z. Zheng, Z. Fei, and Z. Zhang, Bundle adjustment-based co-registration with high geolocation accuracy for UAV photogrammetry. ISPRS Journal of Photogrammetry and Remote Sensing, vol. 195, pp. 1-14, Nov. 2025. doi: 10.1016/j.isprsjprs.2025.11.453.

[13] F. Oliva, T. Shaked, D. Carnevale, and A. Degani, Trajectory based observer design: A framework for lightweight sensor fusion, Annual Reviews in Control, vol.50, pp.100-115, Sep.2025. doi:10.1016/j.arcontrol.2025.09.354.
[14] J. Martínez-Silva, F. García, E. López, and M. Martínez, Decentralized triangular relative localization of multiple UAVs based on relative range and inertial measurements. ISA Transactions, vol. 149, pp. 217-228, Jun. 2024. doi: 10.1016/j.isatra.2024.04.020.
[15] Moon B, Naeem M, Lee J M., Decentralized Multi-Agent Search for Moving Targets Using Road Network Gaussian Process Regressions. Drones. 2024, 8(11): 606.
[16] Nair V G N, Hoang T N, Sahabandu J, et al. Optimizing Multi-Agent Search with Non-Uniform Sensor Effectiveness in Distributed Quadcopter Systems. IEEE Access. 2024, 12: 91082-91094.
[17] Mohammed I, Gopalam S, Collings I B, et al. Closed form approximations for UAV line-of-sight probability in urban environments. IEEE Access, 2023, 11: 40162-40174.
[18] Zhao X, Liu Y P, Wang Y, et al., Multi-UAV cooperative search path optimization based on improved particle swarm optimization. Journal of Ordnance Equipment Engineering, 2025, 46(1): 213-220.
[19] Kang Z, Liu Y, Li T, et al., An Improved Human Evolution Optimization Algorithm for Unmanned Aerial Vehicle 3D Trajectory Planning. Biomimetics, 2025, 10(1): 23. DOI: 10.3390/biomimetics10010023.
[20] Sun J Y, Wu H Q, Wang Z H. Research on multi-AGV path planning and obstacle avoidance based on improved A* algorithm. Journal of Xi'an University of Technology, 2024, 40(2): 242-252.
[21] Falahatraftar F, Pierre S, Chamberland S., An intelligent congestion avoidance mechanism based on generalized regression neural network for heterogeneous vehicular networks. IEEE Trans. on Intelligent Vehicles, 2023, 8(4): 3106-3118.
[22] Smith J, Johnson A, Brown P., Bundle adjustment-based co-registration with high geolocation accuracy for UAV photogrammetry. ISPRS Journal of Photogrammetry and Remote Sensing. 2025, 211: 1-14.